Proc. Natl. Acad. Sci. USA
Vol. 96, pp. 6060–6063, May 1999
Biochemistry

Fire–diffuse–fire model of dynamics of intracellular calcium waves

SILVINA PONCE DAWSON*, JOEL KEIZER†, AND JOHN E. PEARSON†§

*Departamento de Física Facultad de Ciencias Exactas y Naturales, Ciudad Universitaria, Pabellón I, 1428 Buenos Aires, Argentina; †Institute of Theoretical Dynamics & Neurobiology, Physiology, and Behavior, University of California, Davis, CA 95616; and ‡XCM MS F645, Computational Science Methods, Applied Theoretical Physics Division, Los Alamos National Laboratory, Los Alamos, NM 87545

Communicated by Harry L. Swinney, University of Texas, Austin, TX, January 28, 1999 (received for review August 20, 1998)

ABSTRACT **When Ca^{2+} is released from internal stores in living cells, the resulting wave of increased concentration can travel without deformation (continuous propagation) or with burst-like behavior (saltatory propagation). We analyze the "fire–diffuse–fire" model in order to illuminate the differences between these two modes of propagation. We show that the Ca^{2+} release wave in immature *Xenopus* oocytes and cardiac myocytes is saltatory, whereas the fertilization wave in the mature oocyte is continuous.**

Traveling waves in living cells can vary greatly in their appearance. For example, the calcium wave in immature *Xenopus* frog eggs propagates as a sequence of bursts (1–4) (Fig. 1*a*), whereas the calcium wave that occurs during fertilization in mature *Xenopus* eggs appears to be continuous (5, 6) (Fig. 1*b*). It is commonly believed that information is encoded in the time course of the Ca^{2+} signal (7–12). Thus, the distinction between these two modes of propagation likely has physiological significance. Remarkably, the waves in both cell types involve the release of calcium from internal stores via mechanisms that are physically and biologically similar.

We report here a simple physical model that allows us to characterize these behaviors as limiting cases. A prominent feature of this model is the existence of a new time scale in addition to the usual chemical time scales, namely the intersite diffusion time, d^2/D. (Here, D is the diffusion coefficient and d is the source separation.) If intersite diffusion is rate-limiting, the wave will exhibit burst-like (or saltatory) behavior (Figs. 1*a* and 2*a*). If chemical processes are rate-limiting (i.e., slow compared to intersite diffusion), then the resulting wave will be smooth (Figs. 1*b* and 2*b*). Although the intersite diffusion time is likely to be important for other wave phenomena, our analysis of recent experiments suggests that it is an essential feature for intracellular Ca^{2+} waves.

Ca^{2+} is stored intracellularly in the endoplasmic or sarcoplasmic reticulum at 2–3 orders of magnitude greater than its concentration in the cytosol and is released by a process referred to as Ca^{2+}-induced Ca^{2+} release (CICR). CICR involves Ca^{2+} release through specialized Ca^{2+} channels that are activated at slightly elevated levels of cytosolic Ca^{2+} and then inactivated as the level of Ca^{2+} rises further. After an open channel closes via inactivation, it cannot reopen for some time, during which it is in a "refractory" state. Calcium release provides a mechanism for wave propagation (10–17), whereas inactivation limits the amount released.

High-resolution imaging of Ca^{2+} in a variety of cell types reveals localized release events called "puffs" (1–4) (Fig. 1*a*), "sparks" (19), or "quantum emission domains" (8, 9). These events have been correlated with Ca^{2+} release from either individual or small clusters of channels. In muscle cells, sparks are observed at the t-tubule structures in the sarcoplasmic reticulum (20), which are aligned in regular arrays with a characteristic separation of $\sim 2\ \mu$m. In other cell types, inositol trisphosphate stimulates Ca^{2+} release from clusters of inositol triphosphate receptors from the endoplasmic reticulum. Although these inositol triphosphate-dependent sites appear to be randomly distributed, they are characterized by a mean separation (1–4, 21). The release events are the elementary processes underlying Ca^{2+} waves.

Our description of these events is called the "fire–diffuse–fire" model. This model reproduces the full range of wave propagation, from saltatory (Fig. 2*a*) to continuous (Fig. 2*b*). In contrast, homogeneous reaction diffusion models predict only continuous propagation with a velocity (v) proportional to $\sqrt{D/\tau}$, with τ the time scale of a chemical process. When applied to Ca^{2+} waves, the fire–diffuse–fire model predicts that the fertilization wave in *Xenopus* eggs is continuous. Moreover, it shows, in agreement with experiment, that waves in immature *Xenopus* oocytes (1–4) and in cardiac myocytes are saltatory.

The fire–diffuse–fire model consists of a regular array of point-source release sites with spacing, d, embedded in a continuum in which calcium ions diffuse. A related model, in which the discrete entities are individual cells, has been used for modeling cAMP (22) waves. In cells in which release sites do not occur in regular arrays, d should be thought of as a mean spacing. The pumps that resequester the ions back into the stores operate on a somewhat slower time scale (23) and are neglected here for simplicity. Whenever the cytosolic Ca^{2+} concentration in the vicinity of a release site reaches a threshold value, $[Ca^{2+}]_T$, the site begins releasing Ca^{2+} ions at a rate σ/τ. It remains open for a time τ, and then closes after having released a quantity, σ, of Ca^{2+}. Because the binding time for Ca^{2+} with immobile buffers is faster than the other time scales in the problem (15), we treat the action of the Ca^{2+} buffers as instantaneous. To account for the effect of buffering, we define σ as the total amount of Ca^{2+} released divided by a buffering factor of $\sim$100. We use the data in ref. 24 for the buffered diffusion coefficient in *Xenopus* oocytes. Note that this means that both σ and the diffusion coefficient, D, inherit the temperature dependence of the buffering factor.

The processes of Ca^{2+} release (or firing) and diffusion can be described by a single evolution equation described in detail in the *Appendix* and in ref. 25. The dynamics depends on two dimensionless parameters, Γ and β. The first is defined as

$$\Gamma = \frac{(\sigma/d^3)}{[Ca^{2+}]_T - [Ca^{2+}]_b}, \qquad [1]$$

where $[Ca^{2+}]_b$ is the basal Ca^{2+} concentration. The quantity σ/d^3 is the release concentration, since it is the amount of Ca^{2+} released per site after buffering (σ) divided by the volume per site ($1/d^3$). So Γ is the ratio of the release concentration to the difference between basal and threshold concentrations. The parameter β is the ratio of the time a site remains open, τ, to the intersite diffusion time, d^2/D, i.e.

The publication costs of this article were defrayed in part by page charge payment. This article must therefore be hereby marked "*advertisement*" in accordance with 18 U.S.C. §1734 solely to indicate this fact.

PNAS is available online at www.pnas.org.

†To whom reprint requests should be addressed. e-mail: pearson@lanl.gov.

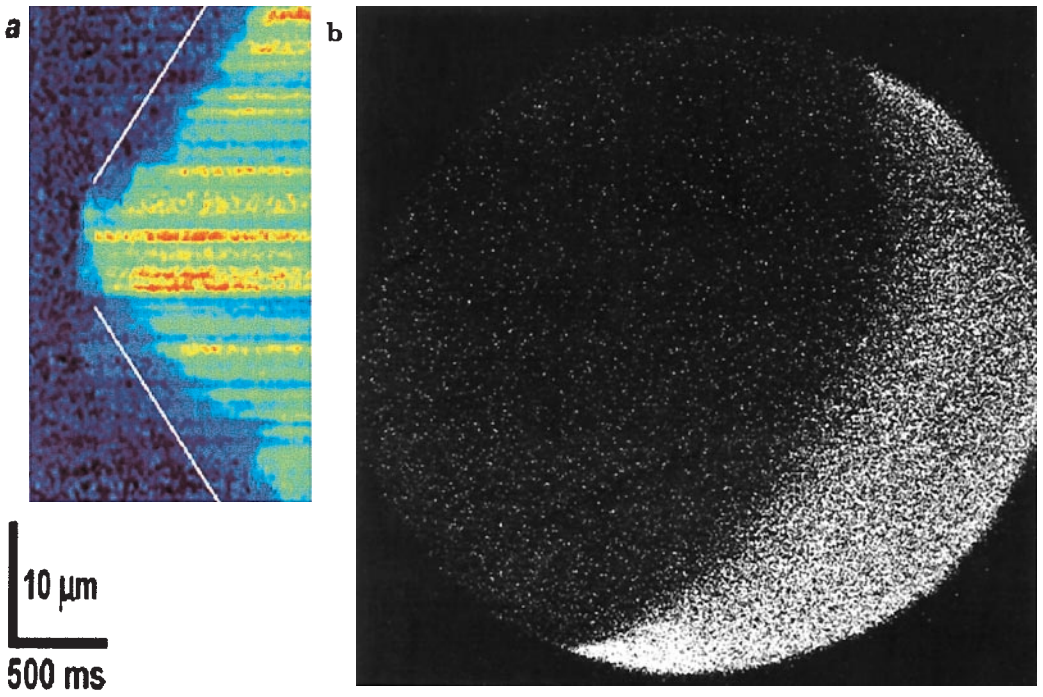

FIG. 1. (*a*) Space–time (or "waterfall") plot of the calcium wave in an immature *Xenopus* oocyte. The image was obtained with high-resolution confocal microscopy (1). "Warmer" colors indicate elevated calcium levels. The individual release sites are clearly visible as streaks. (*b*) Relatively low-resolution snapshot of the calcium fertilization wave in mature *Xenopus* oocyte (5). The lighter region corresponds to higher calcium concentration, which is propagating into the region of lower calcium concentration, i.e., the wave is propagating to the left and up. The diameter is 1.2 mm. The front is ~50 μm deep. If the mean site spacing is 2 μm, then the zone in which calcium is actively being released (i.e., the front) is ~25 sites deep. The resolution is too low to see individual sites. One of the predictions of the fire–diffuse–fire model is that even with the spatial resolution of *a*, it would not be possible to see the individual sites because the release rate is so slow that the calcium diffuses away before significant local buildup can occur. The tiny local buildups that do occur are statistical in nature.

$$\beta = \frac{D\tau}{d^2}. \qquad [2]$$

If release is the rate-limiting process, then $\beta \gg 1$, and the waves are continuous. If intersite diffusion is the rate-limiting process, then $\beta \ll 1$, and the waves are saltatory (25).

A traveling saltatory wave solution ($\beta = 0.08$ and $\Gamma = 3.05$) to the fire–diffuse–fire model is illustrated in Fig. 2*a*. The vertical axis is the Ca^{2+} concentration, and the horizontal axis is position in site spacing units. The parameters were estimated from the literature on the immature oocyte (1–4, 26). The wave is traveling to the right with a velocity of 20 μm/s. Well behind the front (i.e., for $x < \sim 2$), the concentration is $[Ca^{2+}](x, t) = \sigma/d^3 + [Ca^{2+}]_b = 0.66$ μM. The time at which site n begins to fire (i.e., to release Ca^{2+}) is denoted by t_n. The first profile in the sequence is the solid line with the short spike above site 5. This profile occurs just after the Ca^{2+} concentration at site 5 crosses threshold at time $t = t_5$. The second profile in the sequence is the long-dashed line with the tall peak above site 5. This is the profile at time $t = t_5 + \tau$. The peak is wider because of diffusion and higher because the total amount (σ) of Ca^{2+} ions have been released at this time. The third profile is the short-dashed line and corresponds to a time halfway between t_5 and t_6 (after site 5 has completed firing, but before site 6 has reached threshold). The fourth profile is the solid line with the short spike above site 6. This is the profile just after the Ca^{2+} concentration reaches threshold at time $t = t_6$. We see that saltatory propagation consists of a distinct emission of Ca^{2+} when a particular site fires. Obviously, both Ca^{2+} release and Ca^{2+} diffusion occur simultaneously, but the firing time τ is so short compared to the intersite diffusion time, d^2/D, that during the time that a single site is firing, very few ions diffuse to the next site. The shorthand description of these processes, fire–diffuse–fire, is thus an accurate description of the sequence of events shown in Fig. 2*a*.

Continuous propagation ($\beta = 50$ and $\Gamma = 5$) is illustrated in Fig. 2*b*. The parameters in this case are appropriate for the fertilization wave in mature *Xenopus* eggs (5). For D, we used a higher value ($D = 50$ $\mu m^2/s$ because the Ca^{2+} concentration is higher, thus implying less buffering in the egg (24). The wave is traveling to the right with a velocity of 5.2 μm/s. The experimental observations provide the concentration in the wave back, from which it is possible only to estimate σ/d^3 but not σ and d separately. Here, $D\tau = 450$ μm^2. Thus, $\beta = D\tau/d^2$ will be in the range 28–450 for d in the range 1–4 μm. In Fig. 2*b*, we used $d = 3$ μm. These values of β are large enough so that the propagation is continuous. In this regime, the velocity does not depend strongly on d provided $\Gamma = 5$ is fixed. Decreasing d to 1 μm (while decreasing σ by a factor of 27, so that σ/d^3 remains constant) results in a solution that is indistinguishable from the one in Fig. 2*b*, which shows the wave profile at two different times. It travels nearly without deformation.

For steady propagation, we have derived a relationship (25) of the form

$$\Gamma = F(\eta, \zeta), \qquad [3]$$

where ζ and η are dimensionless velocities

$$\zeta \equiv v\sqrt{\tau/D} \qquad [4]$$

and

$$\eta \equiv vd/D. \qquad [5]$$

Combining Eqs. **2**, **4**, and **5**, it follows that

$$\zeta = \sqrt{\beta}\eta. \qquad [6]$$

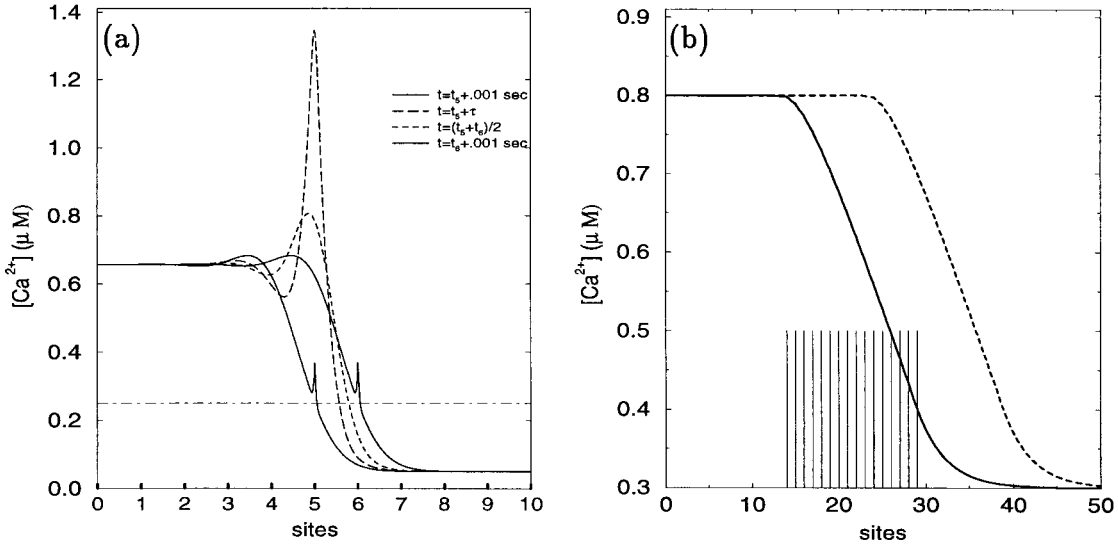

FIG. 2. (*a*) Four snapshots of a rightward saltatory wave solution of the fire–diffuse–fire model. The dashed line denotes the threshold concentration, $[Ca^{2+}]_T$. The values used here were taken from the literature on the immature *Xenopus* oocyte (1–4): $d = 3.9$ μm, $\tau = 0.05$ s, $D = 25$ $\mu m^2/s$ $[Ca^{2+}]_T = 0.25$ μM, $[Ca^{2+}]_b = 0.05$ μM, and $\sigma = 3.5 \times 10^{-14}$ μmol. The wave is traveling to the right with a velocity of 20 μm/s. Note that only one site fires at a time and that the shape of the wave changes with time. (*b*) Two snapshots of a rightward continuous wave. The vertical lines indicate the sites that are simultaneously firing at the time of the first snapshot (solid line). The dashed line corresponds to a later time. The parameters used here were taken from the literature on the fertilization wave in *Xenopus* eggs (5). The values we used correspond to the interior region of the egg: $d = 3$ μm, $D = 50$ $\mu m^2/s$, $\tau = 9$ s, $\sigma = 1.35 \times 10^{-14}$ μmol, $[Ca^{2+}]_T = 0.4$ μM, and $[Ca^{2+}]_b = 0.3$ μM. The wave is traveling to the right with a velocity of 5.2 μm/s. Note that many sites are firing simultaneously and that the wave travels without observable deformation. Despite the larger diffusion coefficient, the continuum wave is slower than the saltatory wave. This is because of the difference in release rates (τ).

It can be shown that $F \geq 1$ so that there is no solution to Eq. **3** if $\Gamma < 1$. This corresponds to the intuition that waves will not propagate if the release concentration is not sufficient to bring the neighboring sites up to threshold. In myocytes, the diffusion constant of Ca^{2+} is of the order of $D = 30$ $\mu m^2\ s^{-1}$, $d \approx 2$ μm, $\tau \approx 15$ *m*s, and $[Ca^{2+}]_T \approx 0.2$ μM (24, 28). Under conditions in which isolated sparks are found experimentally, the unitary Ca^{2+} current at a release site is estimated to be $2pA$ (13, 16), so that including the buffering, we find $\sigma \approx 1.5 \times 10^{-15}$ μmol. Using Eqs. **1** and **2**, this gives $\Gamma \approx 1$ and $\beta \approx 0.1$, in agreement with the observation that waves do not propagate under these conditions. We have shown for the extreme saltatory limit ($\tau \to 0$) that the fire–diffuse–fire model undergoes a series of bifurcations and crises that lead to chaos as propagation failure is approached (i.e., as Γ is decreased) (25, 28). The general feature of complex dynamics should be observed whenever such a system is driven towards propagation failure. On the other hand, waves do propagate in myocytes under conditions of Ca^{2+} overload (20), which increases the unitary current, thus increasing Γ. Simulations and more detailed calculations (27, 28) suggest that $\Gamma \approx 5$. This generates waves with the experimentally observed velocity of about 65 μm/s, and since $\beta \approx 0.1$, these waves are saltatory, in agreement with experiment.

Although the explicit form of F in terms of η and ζ is complicated (25), the resulting function is simple. Fig. 3 is a contour plot of $F(\eta, \zeta)$ upon which are superimposed straight lines $\zeta = \sqrt{\beta}\eta$ for several values of β. Any two of the quantities Γ, β, η, and ζ, when different from zero, determine the other two.

If $\zeta^2/\eta \ll 1$ (which holds for small enough β) the propagation is saltatory. In this case, F can be approximated by a function of η only so that Eq. **3** reduces to $F(\eta, 0) \equiv g(\eta) = \Gamma$ from which we find that $\eta = g^{-1}(\Gamma)$ so that

$$v \approx \frac{D}{d} g^{-1}(\Gamma). \qquad [7]$$

Here, g^{-1} denotes the inverse function of g. If Γ is large enough, we get an approximate explicit formula for g^{-1} which gives $v \approx 4D/d\log\Gamma$. If $\zeta^2/\eta \gg 1$ and $\beta \gg 1$, propagation is continuous. In this case, F can be approximated by a function of ζ only so that Eq. **3** reduces to $F(0, \zeta) \equiv f(\zeta) = \Gamma$, from which we find that $\zeta = f^{-1}(\Gamma)$ so that

$$v \approx \sqrt{\frac{D}{\tau}} f^{-1}(\Gamma). \qquad [8]$$

Here, if Γ is large enough, we get an approximate explicit formula for f^{-1} that gives $v \approx \sqrt{\Gamma}\sqrt{D/\tau}$. This is Luther's equation (15, 16) ($v = \alpha\sqrt{D/\tau}$) with $\alpha = \sqrt{\Gamma}$. For the continuous-fertilization Ca^{2+} wave in Fig. 1*b*, $\Gamma = 5$, and this approximation is accurate to within a few percent. It is, however, completely incorrect for saltatory waves.

Typically, propagation is saltatory if $\beta \ll 1$ and continuous if $\beta \gg 1$. Given a value of Γ, it is clear from Fig. 3 that for small enough β the intersection between the line $\zeta = \sqrt{\beta}\eta$ and the contour will occur at values that satisfy $\zeta^2/\eta \ll 1$. This is the saltatory case. On the other hand, for large enough β, the intersection will occur at values that satisfy $\zeta^2/\eta \gg 1$. This is the continuous case. One of the most distinctive physical differences between continuous and saltatory waves is the number of sites that are simultaneously firing. This is given by $1 + v\tau/d = 1 + \zeta^2/\eta$. The curve $\eta = \zeta^2$ is shown as the dashed line in Fig. 3. Data points lying below this curve have only a single site firing at a time and those above have two or more. As illustrated by the vertical lines in Fig. 2*b*, many sites fire simultaneously during continuous propagation. On the other hand, as shown in Fig. 2*a*, only a single site fires at a time during saltatory propagation. More detailed models will share this and other general features of the fire–diffuse–fire model. Thus, whether a wave is saltatory or continuous will be determined by β. The trend of increasing velocity with increasing release concentration and the approach to propagation failure as the release density is decreased will both hold.

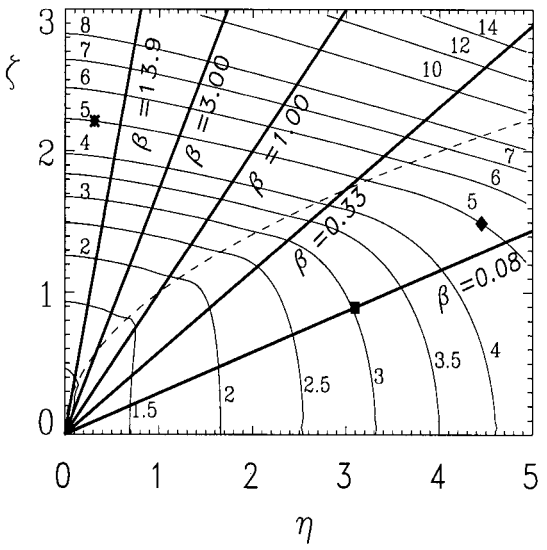

FIG. 3. Contour plot of $F(\eta, \zeta)$ with straight lines $\zeta = \sqrt{\beta}\eta$ superimposed. The dashed line is the line $\eta = \zeta^2$. *, ■, and ◆ denote three of the cases discussed in the text: the mature oocyte, the immature oocyte, and the myocyte in overload, respectively. The latter two are such that $\eta > \zeta^2$ and thus correspond to saltatory waves. For *, $\eta \ll \zeta^2$, and the propagation is continuous.

The parameter values used here for oocytes, myocytes, and eggs are within experimentally accepted ranges. However, the specific values were chosen to reproduce the experimental velocities. Other values within the experimentally observed range give velocities that are off by as much as a factor of 5. The match (or mismatch) between experimentally observed and theoretically predicted velocities cannot be used either to validate or to invalidate a particular model. For example, using the Luther equation as in refs. 15 and 16 ($v = \sqrt{D/\tau}$) gives a velocity of 22 μm/s for the waves in the immature oocyte as in Fig. 2*a*. These values ($D = 25\ \mu m^2/s$, $\tau = 0.05$s, and $v = 22\mu$/s) are all within the experimental uncertainty. However, the Luther equation is manifestly wrong since the wave is saltatory (1,2). Decreasing τ by a factor of 50 in Fig. 2*a* results in a change in v of only a few percent, whereas the Luther equation yields a velocity of 160 μm/s! The fact that $\sqrt{D/\tau}$ is approximately equal to the velocity of the model saltatory wave is purely coincidental.

Whether the mode of propagation is continuous or saltatory is at least as important a fact as the numerical value of the velocity. Our analysis provides a simple, robust prescription for predicting the mode of propagation: estimate β. If estimates of β are all <0.1, it is safe to assume that propagation is saltatory; if they are >10, propagation is continuous. For intermediate values of β ($0.1 \leq \beta \leq 10$), a more accurate model (namely, ref. 25) would be necessary to determine the mode of propagation. As it is widely held that information is encoded in the Ca^{2+} signal (7–12), the distinction between saltatory and continuous waves likely has considerable physiological significance.

The fire–diffuse–fire model of calcium propagation is described by the single-evolution equation

$$\frac{\partial[Ca^{2+}]}{\partial t} = D\frac{\partial^2[Ca^{2+}]}{\partial^2 x} + \frac{\sigma}{d^2\tau}\sum_{i=-\infty}\delta(x - x_i)H(t - t_i)H(t_i + \tau - t), \quad \textbf{[9]}$$

where $[Ca^{2+}](x, t)$ is the average concentration of calcium in the directions perpendicular to that of propagation (x), $\delta(\zeta)$ is the δ function, $H(\zeta)$ is the Heaviside step function [$H(\zeta) = 0$ for $\zeta < 0$, $H(\zeta) = 1$ for $\zeta \geq 0$], D is the diffusion coefficient of calcium, t_i is the first time at which the ith site takes on the threshold value, $[Ca^{2+}]_T$, σ is the total number of ions released by a site, and τ is the "rise time" for the receptor (i.e., the length of time the receptor is open during a release event). The δ function density for the receptors means we are treating the receptor/channels as point sources. As stated in the text, the binding to buffers is assumed instantaneous. Thus, the effect of buffering is reflected in the values used for D and σ. Details can be found at http://www-xdiv.lanl.gov/XCM/pearson/fdf.

This work was supported by National Institutes of Health Grant R01 RR10081 to J.K. and the Agricultural Experiment Station at University of California Davis. S.P.-D. was supported by the University of Buenos Aires, Consejo Nacional de Investigaciones Científicas y Técnicas de Argentina (CONICET), and Fundación Antorchas. J.E.P. was supported by the Los Alamos National Laboratory Lab Directed Research and Development (LDRD) program. This work was partially motivated by a conversation that one of us (J.E.P.) had with Jim Keener. We thank Bob Silver, Gregory Smith, Lionel Jaffe, and Werner Horsthemke for helpful conversations. We would especially like to thank I. Parker and R. Nuccitelli for useful conversations and for providing figures 1*a* (Parker) and 1*b* (Nuccitelli).

1. Callamaras, N., Marchant, J. S., Sun, X.-P., and Parker, I. (1998) *J. Physiol.* **509,** 81–91.
2. Parker, I. & Yao, Y. (1991) *Proc. R. Soc. London B* **246,** 269–274.
3. Parker, I., Choi, J. & Yao, Y. (1996) *Cell Calcium* **20,** 105–121.
4. Yao, Y., Choi, J. & Parker, I. (1994) *J. Physiol. (London)* **482,** 533–553.
5. Fontanilla, R. A. & Nuccitelli, R. (1998) *Biophys. J.* **75,** 2079–2087.
6. Nuccitelli, R., Yim, D. L. & Smart, T. (1993) *Dev. Biol.,* **158,** 200–212.
7. de Koninck, P. & Schulman, H. (1998) *Science,* **279,** 227–230.
8. Llinas, R., Sugimori, M. & Silver, R. B. (1992) *Science* **256,** 677–679.
9. Silver, R. B. (1996) *Cell Calcium* **20,** 161–179.
10. Lechleiter, J., Girard, S., Peralta, E. & Clapham, D. (1991) *Science* **252,** 123–126.
11. Lechleiter, J. & Clapham, D. (1992) *Cell* **69,** 283–294.
12. Atri, A., Admunson, J., Clapham, D. & Sneyd, J. (1993) *Biophys. J.* **65,** 1727–1739.
13. Dupont, G. & Goldbeter, A. (1992) *Biophys. J.* **67,** 2191–2204.
14. Jafri, M. S. & Keizer, J. (1995) *Biophys. J.* **69,** 2139–2153.
15. Jaffe, L. (1993) *Cell Calcium* **14,** 736–745.
16. Jaffe, L. (1991) *Proc. Natl. Acad. Sci. USA* **88,** 9883–9887.
17. Berridge, M. J. (1993) *Nature (London)* **361,** 315–325.
18. Bootman, M. & Berridge, M., (1995) *Cell* **83,** 675–678.
19. Cheng, H., Lederer, W. J. & Cannell, M. B. (1993) *Science* **262,** 740–744.
20. Cheng, H., Lederer, M. R., Lederer, W. J. & Cannell, M. B. (1996) *Am. J. Physiol.* **39,** C148–C159.
21. Horne, J. H. & Meyer, T. (1997) *Science* **276,** 1690–1693.
22. Levine, H., Aranson, I., Tsimring, L. & Truong, T. V. (1996) *Proc. Natl. Acad. Sci. USA* **93,** 6382–6386.
23. Smith, G. D., Keizer, J. E., Stern, M. D., Lederer, W. J. & Cheng, H. (1998) *Biophys. J.* **75,** 15–32.
24. Allbritton, N. L., Meyer, T. & Stryer, L. (1992) *Science* **258,** 1812–1815.
25. Pearson, J. E. & Ponce-Dawson, S. (1997) *Physica A (Amsterdam)* **257,** 141–148.
26. Kaftan, E. J., Ehrlich, B. E. & Watras, J. (1997) *J. Gen. Physiol.* **110,** 529–538.
27. Keizer, J. & Smith, G. D. (1998) *Biophys. Chem.* **72,** 87–100.
28. Keizer, J., Smith, G. D., Ponce-Dawson, S. & Pearson, J. (1998) *Biophys. J.* **75,** 595–600.